




RESEARCH ARTICLE

QSM is an imaging biomarker for chronic glial activation in multiple sclerosis lesions

Kelly M. Gillen¹ , Mayyan Mubarak², Calvin Park², Gerald Ponath², Shun Zhang¹, Alexey Dimov¹, Maya Levine-Ritterman², Steven Toro², Weiyuan Huang¹, Stephanie Amici³, Ulrike W. Kaunzner⁴, Susan A. Gauthier^{1,4} , Mireia Guerau-de-Arellano³, Yi Wang¹, Thanh D. Nguyen¹ & David Pitt² 

¹Department of Radiology, Weill Cornell Medicine, New York, New York

²Department of Neurology, Yale School of Medicine, New Haven, Connecticut

³Department of Neuroscience, The Ohio State University, Columbus, Ohio

⁴Department of Neurology, Weill Cornell Medicine, New York, New York

Correspondence

David Pitt, Department of Neurology, Yale School of Medicine, 300 George St., Suite 353 I, New Haven, CT 06511. Tel: +1 (203) 737-7951; E-mail: David.pitt@yale.edu

Received: 17 December 2020; Revised: 18 February 2021; Accepted: 22 February 2021

Annals of Clinical and Translational Neurology 2021; 8(4): 877–886

doi: 10.1002/acn3.51338

Abstract

Background: Inflammation in chronic active lesions occurs behind a closed blood–brain barrier and cannot be detected with MRI. Activated microglia are highly enriched for iron and can be visualized with quantitative susceptibility mapping (QSM), an MRI technique used to delineate iron. **Objective:** To characterize the histopathological correlates of different QSM hyperintensity patterns in MS lesions. **Methods:** MS brain slabs were imaged with MRI and QSM, and processed for histology. Immunolabeled cells were quantified in the lesion rim, center, and adjacent normal-appearing white matter (NAWM). Iron⁺ myeloid cell densities at the rims were correlated with susceptibilities. Human-induced pluripotent stem cell (iPSC)-derived microglia were used to determine the effect of iron on the production of reactive oxygen species (ROS) and pro-inflammatory cytokines. **Results:** QSM hyperintensity at the lesion perimeter correlated with activated iron⁺ myeloid cells in the rim and NAWM. Lesions with high punctate or homogenous QSM signal contained no or minimally activated iron⁻ myeloid cells. In vitro, iron accumulation was highest in M1-polarized human iPSC-derived microglia, but it did not enhance ROS or cytokine production. **Conclusion:** A high QSM signal outlining the lesion rim but not punctate signal in the center is a biomarker for chronic inflammation in white matter lesions.

Introduction

A pathological hallmark of MS is acute inflammatory demyelination of white matter. Because demyelination is associated with the breakdown of the blood–brain barrier (BBB), acute lesions can be visualized with an accumulation of gadolinium (Gd). In contrast, chronic inflammation in the perimeter of established lesions takes place behind a closed BBB and cannot be detected with conventional MRI. We and others have shown that smoldering innate inflammation in chronic active lesions is associated with iron accumulation within microglia and post-demyelinating macrophages.^{1–5}

Iron can be visualized and quantified with QSM, an MRI technique that exploits tissue susceptibilities. Tissue

becomes magnetized in response to a magnetic field that arises from unpaired electrons in iron or external sources such as contrast agent; the extent of this magnetization is known as susceptibility.⁶ QSM increases in response to iron accumulation and loss of myelin, and has several in vivo applications such as quantifying iron overload in Parkinson's disease⁷ and amyotrophic lateral sclerosis,⁸ and visualization of subthalamic nuclei for deep brain stimulation.⁹ In MS patients, QSM studies have shown distinct susceptibility patterns in a subpopulation of white matter lesions, including lesions with hyperintense rims.^{2,10–13} Moreover, we have established a timeline for susceptibility changes in developing white matter lesions in retrospective and ongoing prospective studies.^{11,14} We found that tissue susceptibility in early, Gd-enhancing

white matter lesions are isointense, increases rapidly after enhancement, plateaus, and decays slowly to levels similar to that of NAWM over an average of 6–8 years.¹⁴ The long-term persistence of iron-related inflammation in the perimeter of established lesions suggests an important role for chronically activated, iron⁺ myeloid cells in MS pathogenesis.

Here we combined QSM with subsequent histological evaluation of MS autopsy tissue to (1) demonstrate quantitatively that high QSM signal at the lesion rim correlates with iron⁺ myeloid cells, (2) identify the histological correlates of QSM patterns, and (3) characterize the activation states of iron⁺ and iron⁻ myeloid cells in situ and in vitro.

Materials and Methods

Postmortem experiments

MS tissue

We obtained from the Rocky Mountain MS Center Tissue Bank formalin-fixed coronal brain slabs from 16 MS patients. All lesions included in this study were located in the periventricular and deep white matter of the cerebrum; lesions from the optic nerve, brain stem, cerebellum, and spinal cord were excluded. Patient demographics, disease course, and lesion details are listed in Table 1.

MR imaging

Formalin-fixed postmortem brain specimens were embedded in 1% agarose and scanned on 3T clinical MRI scanners (GE Healthcare, Milwaukee, WI; SIEMENS, Erlangen) using the product head coil. The typical imaging protocol consisted of 2D T2-weighted fast spin echo sequence (voxel size = $0.5 \times 0.5 \times 1.0 \text{ mm}^3$, TE = 57 msec, TR = 6.8 sec, readout bandwidth (rBW) = 195 Hz/pixel, echo train length = 23, number of signal averaging = 6) for lesion identification, and 3D multi-echo gradient echo (GRE) sequence (voxel size = $0.5 \times 0.5 \times 0.5 \text{ mm}^3$, first TE = 3.7 msec, ΔTE = 6.6 msec, TR = 42 msec, flip angle = 20 degrees, rBW = 163 Hz/pixel) for QSM. QSM images were reconstructed using morphology enabled dipole inversion.¹⁵

Lesion classification

White matter lesions were classified on QSM by SZ and WH; UK and SAG resolved any disagreements. We identified MS lesions based on T2FLAIR hyperintensity, and then used the corresponding QSM images to classify lesions as hyperintense, hypointense, or isointense on QSM.

Hyperintense lesions on QSM were characterized as having susceptibility greater than surrounding normal-appearing white matter. Hypointense lesions on QSM were defined as having susceptibility lower than that of surrounding normal-appearing white matter. Isointense lesions were indistinguishable on QSM because their susceptibility was equal to that of normal-appearing white matter. The different patterns of hyperintensities include (1) low grade, homogeneous susceptibility in the lesion center, (2) high susceptibility puncta in the lesion center, and (3) hyperintense lesion rim. All QSM hyperintense lesions displayed low-grade homogeneous susceptibility in the center, which is presumably caused by the absence of myelin. In addition, some lesions displayed high susceptibility puncta within the lesion center and high susceptibility at the lesion rim. In order to determine the susceptibility in the center (either low-grade homogeneous or high susceptibility puncta), we segmented the lesion center. In order to quantify susceptibility in the lesion rim, we segmented the lesion rim. QSM measurements were obtained using ITK-SNAP (version 3.8.0; <http://itksnap.org/>).

Immunohistochemistry

After MRI, lesions were excised, embedded in paraffin, and cut into 5 μm sections. Sections were deparaffinized in xylene, rehydrated, and antigen retrieval was performed with 10mM sodium citrate buffer (pH 6) for 20 min. Sections were quenched, blocked, and incubated overnight with primary antibodies against myelin basic protein (MBP, Dako A0623, 1:500), CD68 (microglia/macrophages; CellSignaling #76437, 1:500), iNOS (inducible nitric oxide synthase; Novus NB120-15203, 1:300), Ferritin (abcam ab75972, 1:100), CD206 (abcam ab117644, 1:200), and MerTK (tyrosine-protein kinase MER; abcam ab52968, 1:500). Tissue was processed with the appropriate biotinylated secondary antibodies and avidin/biotin staining kit with diaminobenzidine (DAB) as chromogen (Vector Laboratories ABC Elite Kit and DAB Kit). Negative controls included isotype-controls and absence of immunolabeling in tissues that do not express the above antigens. DAB-enhanced Perls' Prussian blue was used to detect ferric iron. Slides were immersed in 4% ferrocyanide/4% hydrochloric acid for 30 min in the dark, and staining was enhanced through incubation with DAB for 30 min at room temperature. After staining, all sections were rinsed, dehydrated, cover-slipped, and digitized using a Mirax digital slide scanner.

Cell counting

Regions of interest (ROIs; $0.3 \pm 0.18 \text{ mm}^2$) were drawn in the lesion center, rim, and NAWM. For each lesion,

Table 1. Patient demographics, disease course, and lesion details.

Case	Age (y)	Sex	PMI (h)	Disease course	Disease duration (y)	T2 lesions	QSM lesion intensity			QSM lesions with histology data Lesion#; QSM pattern (Histology)
							Hypo	Iso	Hyper	
MS 1	46	M	11	RRMS	9	5	0	0	5	L1; Heterogeneous, rim+ (Chronic active, iron+) L2; Heterogeneous, rim+ (Chronic active, iron+) L3; Heterogeneous, rim+ (Chronic active, iron+) L4; Heterogeneous, rim+ (Chronic active, iron+)
MS 2	45	F	20	SPMS	19	20	6	4	10	L1; Heterogeneous, rim- (Chronic active, iron-) L2; Heterogeneous, rim- (Chronic active, iron-) L3; Heterogeneous, rim- (Chronic active, iron-) L4; Heterogeneous, rim- (Chronic silent, iron-)
MS 3	38	M	24	SPMS	8	5	0	0	5	L1; Heterogeneous, rim- (Chronic active, iron-) L2; Heterogeneous, rim+ (Chronic active, iron+) L3; Heterogeneous, rim+ (Chronic active, iron+) L4; Heterogeneous, rim+ (Chronic active, iron+)
MS 4	42	M	5.5	SPMS	12	8	0	0	8	L1; Heterogeneous, rim+ (Chronic active, iron+) L2; Homogeneous, rim- (Acutely demyelinating) L3; Homogeneous, rim+ (Chronic active, iron+)
MS 5	60	F	12	PPMS	Unknown	10	0	0	10	L1; Homogeneous, rim- (Chronic silent, iron-) L2; Heterogeneous, rim- (Chronic active, iron-)
MS 6	63	M	9	SPMS	29	2	0	1	1	L1; Homogeneous, rim- (Chronic silent, iron-)
MS 7	60	M	11	SPMS	18	1	0	0	1	L1; Homogeneous, rim- (Chronic silent, iron-)
MS 8	74	F	7	SPMS	31	3	0	0	3	L1; Homogeneous, rim- (Chronic silent, iron-)
MS 9	36	M	24	RRMS	7	9	1	3	5	N/A
MS10	37	M	19	RRMS	5	9	6	1	2	N/A
MS11	60	F	33	SPMS	25	7	6	1	0	N/A
MS12	61	F	23	SPMS	31	5	1	3	1	N/A
MS13	74	F	24	SPMS	21	3	1	1	1	N/A
MS14	57	F	6	SPMS	29	0	0	0	0	N/A
MS15	72	F	17	SPMS	30	0	0	0	0	N/A
MS16	80	M	17	Stable, chronic	unknown	5	4	0	1	N/A

PMI, post-mortem interval; RRMS, relapsing-remitting multiple sclerosis; PPMS, primary progressive multiple sclerosis; SPMS, secondary progressive multiple sclerosis.

we placed two ROIs in the center, three ROIs in the rim and two ROIs in the NAWM. For lesions with a partial QSM rim, we counted four ROIs in the rim: two ROIs corresponding to regions of high susceptibility and two ROIs in corresponding to regions with low susceptibility. Rims were defined histologically based on the density of CD68⁺ cells at the lesion rim. NAWM ROIs were sampled 0.57 ± 0.24 mm from the outer rim edge in iron⁻ lesions and 1.24 ± 0.52 mm from the outer rim edge in iron⁺ lesions.

DAB-positive cells were counted manually and classified as microglia or macrophage based on morphological appearance, including ramification and soma size by two observers blinded to QSM.¹⁶ Counts were averaged and cell density was calculated based on ROI area. To correct for differences in rim size, linear density (cells/mm) was calculated by multiplying density (cells/mm²) by rim thickness (mm).

Blood vessel quantification

Blood vessels within the lesion that contained $>10,000 \mu\text{m}^2$ area of fixated blood were manually segmented and summed.

In vitro experiments

Generation of microglia cells from induced pluripotent stem cells

Induced pluripotent stem cells (iPSCs) derived from skin biopsies of five healthy donors were differentiated into microglia.¹⁷ Briefly, iPSCs were cultured on matrigel-coated plates in mTeSR1 medium supplemented with Y-27632 (ROCK inhibitor) until 50–60% confluency. Culture medium was switched to customized mTSeR medium (mTSeR1 without LiCl, GABA, Pipicolinic Acid, bFGF, and TGF β 1) supplemented with 80 ng/mL BMP4. The medium

was exchanged daily. After 4 days, the medium was switched to StemPro-34 supplemented with 2 mmol/L Glutamax, 25 ng/mL bFGF, 100 ng/mL SCF, and 80 ng/mL VEGF. After 2 days, the medium was switched to StemPro-34 supplemented with 2 mmol/L Glutamax, 50 ng/mL SCF, 50 ng/mL IL-3, 5 ng/mL TPO, 50 ng/mL M-CSF, and 50 ng/mL Flt-3. After 14 days, floating cells were collected and immature microglia progenitors were purified with anti-CD14 coupled magnetic beads (Miltenyi). Purified progenitors were differentiated into microglia by culturing with RPMI-1640 supplemented with 2 mmol/L Glutamax, 10 ng/mL GM-CSF and 100 ng/mL IL-34, and medium exchange every other day for 14 days. iPSC-derived microglia were polarized toward an M1 phenotype by incubation with LPS (1 mg/mL) and IFN- γ (100 U/mL) or an M2 phenotype with IL-4 (20 ng/mL) for 3 days.¹

Radioactive iron uptake and reactive oxygen species assays

To quantify iron uptake, microglia were cultured with HBSS containing 0.5 μ mol/L iron(III)sulfate and ⁵⁵Fe (1 μ Ci, ferric chloride in 0.5 mol/L HCl; PerkinElmer) at a 100:1 for 24 h at 37 °C. Cells were transferred onto ice, washed twice with ice-cold HBSS, and lysed with 0.1 N NaOH. [⁵⁵Fe] radioactivity was measured using a scintillation counter and counts were normalized to total protein level per sample. ROS generation was assessed by adding 1:5000 CellROX[®] (Life Technologies) 30 min prior to fluorescence measurement in a microplate reader.

Quantitative RT-PCR

Total RNA from iPSC-derived microglial cells was extracted using the miRNeasy[®] Mini Kit (Qiagen). Quantitative real-time PCR was run on a StepOne[™] Real-time PCR system (Life Technologies) and data were analyzed based on the $\Delta\Delta C_T$ method with normalization of the raw data to the HPRT housekeeping gene.

Protein detection

Cytokine release was quantified by Enhanced Sensitivity Cytometric Bead Array (IL10, CXCL10, VEGF, and CCL2; BD Biosciences) or by sandwich ELISAs (DuoSet ELISA for IL6, IL1 β , and TNF α ; R&D Systems). Supernatants were assayed according to the manufacturer's instructions.

Statistical analysis

Data were analyzed by Student's unpaired *t*-test, or one-way ANOVA followed by the Tukey–Kramer multiple comparison test.

Results

Histological correlates of susceptibility patterns of MS lesions on MRI

We imaged 16 brain slabs from 16 MS patients with T2/FLAIR and QSM sequences. On T2/FLAIR, we identified 92 white matter lesions of which 53 (57.6%) contained QSM hyperintense signal. The remaining 39 lesions were isointense ($n = 14$; 15.2%) or hypointense ($n = 25$; 27.2%) with respect to nearby NAWM.

We focused our analyses on the 53 white matter lesions that were hyperintense on QSM. All lesions displayed homogenous susceptibility slightly above that of NAWM (QSM⁺; 13.57 ± 16.28 ppb; Fig. 1A). In addition, we classified QSM⁺ lesions as having a hyperintense lesion rim (58.20 ± 13.84 ppb), a center with hyperintense puncta (23.49 ± 17.18 ppb), or a combination of both. Of the 53 QSM hyperintense lesions, 10 lesions contained both hyperintense rims and hyperintense puncta, 31 lesions contained high susceptibility puncta only, and one lesion had a hyperintense rim but no hyperintense puncta. 11 lesions displayed homogenous susceptibility without hyperintense rim and puncta. High susceptibility puncta were contained predominantly within the lesion area as defined by T2/FLAIR hyperintensities, whereas hyperintense rims were invariably located in the lesion perimeter (Fig. 1B).

We processed 20 of 53 lesions for histochemical and immunohistochemical evaluation. Since QSM signal in the CNS is generated by loss of myelin and an increase in iron, we stained lesion tissue with an antibody against MBP and with Prussian blue (Perls' stain) to detect ferric (Fe³⁺) iron. MBP was absent from all 20 T2/FLAIR hyperintense lesions, consistent with complete demyelination and corresponding to the homogeneous, low-intensity susceptibility pattern on MRI. Moreover, no Perls staining was present in the lesion parenchyma.

Next, we correlated high QSM signal intensity in the rim of 9 lesions ($n = 7$ full rim; $n = 2$ partial rim) with density of Perls' and CD68-positive cells. QSM signal at the lesion rim strongly correlated with iron present in activated microglia ($n = 8$) and reactive astrocytes ($n = 1$) ($r^2 = 0.77$; Fig. 1C). In contrast, 10 QSM rim-negative lesions showed no Perls staining at the lesion rim and exhibited no or only minimally activated microglia. One QSM rim-negative lesion was Perls negative and showed acute demyelination.

Finally, because deoxygenated iron-containing hemoglobin is a strong susceptibility source, we quantified within lesions the number of blood vessels containing fixed blood as well as the total area of vascular blood. The majority of blood vessels were located within the

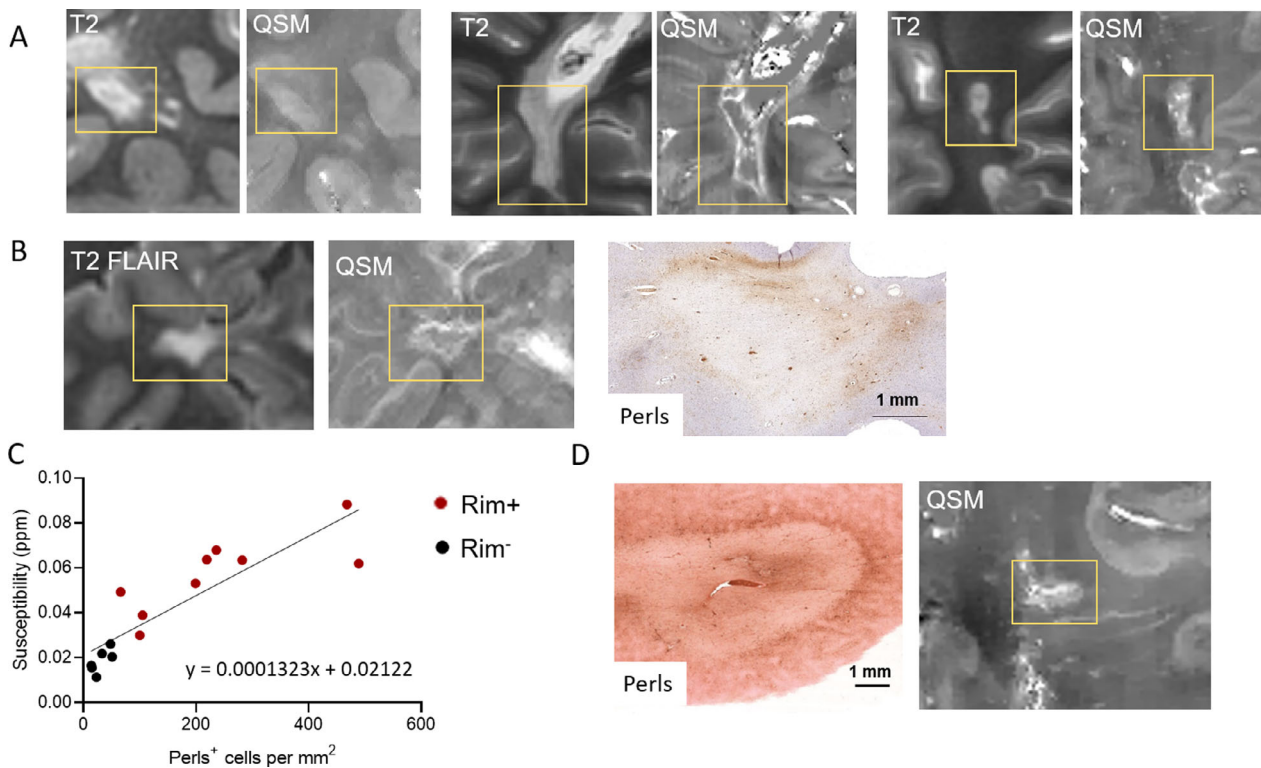


Figure 1. QSM signal accumulates at the lesion rim and correlates with the density of Perl's⁺ cells. (A) Three lesions depicted on T2 and QSM. Left: QSM rim⁻ lesion with homogeneous susceptibility; middle: QSM rim⁺ lesion; right: QSM rim⁻ lesion with high susceptibility puncta. (B) Representative QSM rim⁺ lesion with a hyperintense rim that is located outside of the lesion area as defined by T2 FLAIR (left), and corresponding Perl's stain (right). (C) Increased density of Perl's⁺ cells correlates with increased susceptibility. Red dots represent rim⁺ lesions, black dots represent rim⁻ lesions. (D) Lesion with a central vein partially filled with fixed blood on Perl's stain (left) visible on QSM (right).

lesion center rather than the lesion rim. Moreover, lesions with high susceptibility puncta contained significantly more blood-filled vessels (4.20 ± 4.42 vessels vs. 0.17 ± 0.41 vessels; $p = 0.031$) and a significantly greater area of fixed blood (0.088 ± 0.089 mm² vs. 0.023 ± 0.057 mm²; $p = 0.041$) than lesions without puncta (Fig. 1D).

Myeloid cell distribution, morphology, and marker expression in chronic active lesions

Next, we characterized myeloid cells in QSM rim-positive and rim-negative white matter lesions. Iron⁺ myeloid cells were present in chronic active lesions, with the highest linear density (density (cells/mm²) multiplied by rim thickness (mm)) at the lesion rim (average of 244.5 cells/mm) extending into the NAWM (average of 378.4 cells/mm).

The majority of myeloid cells in the lesion rim had a globoid morphology, whereas a minority exhibited a microglia-like ramified morphology.¹⁸ This ratio

changed toward a higher fraction of ramified cells in the NAWM (Fig. 2A–C and G). Similarly, iron⁺ myeloid cells were predominantly globoid in the lesion rim and predominantly ramified in the NAWM (Fig. 2H). A fraction of QSM rim-negative lesions contained myeloid cells at the rim and adjacent white matter. These cells exhibited a mildly to non-reactive ramified morphology, were substantially less dense (average of 104.6 cells/mm at the rim, and 64.3 cells/mm in the NAWM) and were iron⁻ (Fig. 2D–H). Moreover, the rim and NAWM were substantially larger in iron⁺ than iron⁻ lesions (Fig. 2I).

We further investigated the expression of markers for proinflammatory activation (iNOS, ferritin), iron storage (ferritin), pattern recognition (CD206), and phagocytosis (MerTK)^{19–21} by myeloid cells within the lesion center, rim, and perimeter. All markers were expressed in myeloid cells from iron⁺ lesions, and were absent or substantially less expressed in iron⁻ lesions, indicating that iron⁺ myeloid cells were highly activated, whereas iron⁻ microglia were minimally activated (Fig. 3).

Proinflammatory activation of microglia is associated with iron uptake

We further determined the impact of microglial activation on iron uptake and the effect of iron accumulation on the production of proinflammatory cytokines, using human iPSC-derived microglial cells. Polarization of iPSC-derived microglia with LPS/IFN- γ (M1) and IL-4 (M2) resulted in specific morphological features described in primary mouse microglia (Fig. 4A)¹⁸. Iron uptake was increased in M1 and M0-polarized compared to M2-polarized microglia (Figure 4A and B), in agreement with previously demonstrated preferential iron uptake of LPS-stimulated monocyte-derived macrophages.¹ Iron exposure of unstimulated (M0), TNF α -stimulated, or LPS/IFN- γ -stimulated iPSC-derived microglia did not result in a significantly increased production of ROS or proinflammatory markers (Figure 4D and E).

Discussion

In this study, we combined QSM of autopsied MS lesions with histological analysis to investigate the potential of susceptibility distribution as an imaging biomarker for

chronic inflammation. We observed three separate susceptibility patterns: low grade, homogeneous susceptibility in the lesion center, high susceptibility puncta in the lesion center and hyperintense lesion rim. All QSM hyperintense lesions displayed low-grade homogeneous susceptibility in the center. A subset also contained high susceptibility puncta within the center (termed heterogeneous lesions) and others displayed high susceptibility at the lesions (termed rim positive).

High susceptibility at the rim of white matter lesions was strongly correlated with iron⁺ myeloid cells that reached far into the lesion perimeter, in agreement with other studies.^{2,3} This cellular distribution was consistent with the observation that susceptibility was located outside of lesions as outlined by T2/FLAIR hyperintense signal. Iron⁺ myeloid cells expressed multiple activation markers and displayed a primarily globoid morphology, indicative of a highly activated state. QSM rim-negative lesions either contained no or low numbers of iron⁻ microglia cells that expressed no activation markers. Therefore, activated microglia in chronic active lesions were invariably iron⁺, whereas iron⁻ microglia at the lesion rim were associated with minimal activation. In this study, rim QSM signal was consistently associated

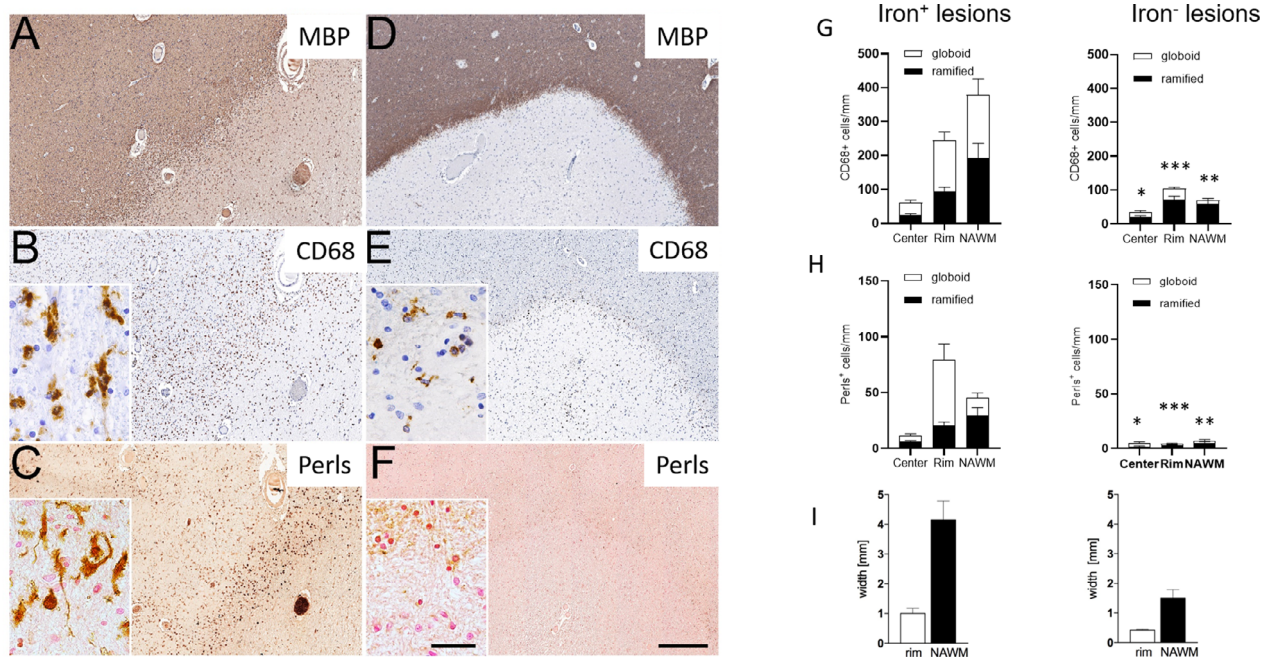


Figure 2. Distribution of myeloid cells in rim⁺ and rim⁻ lesions. A representative rim⁺ lesion with (A) loss of myelin in the lesion center contains (B) a high density of myeloid cells at the lesion rim and (C) Perls⁺ cells with an activated morphology. A representative rim⁻ lesion with (D) complete loss of myelin contains (E) a thin layer of myeloid cells at the lesion rim but (F) lacks Perls⁺ cells. (G–H) Histological quantification. (I) Myeloid cells extend further into the NAWM of iron⁺ lesions as compared to iron⁻ lesions. Bars represent mean + SEM of $n > 10$ ROIs. Average linear density in Center, Rim, NAWM were compared between iron⁺ and iron⁻ lesions to determine statistical significance. MBP, myelin basic protein; * $p < 0.05$; ** $p < 0.01$; *** $p < 0.001$.

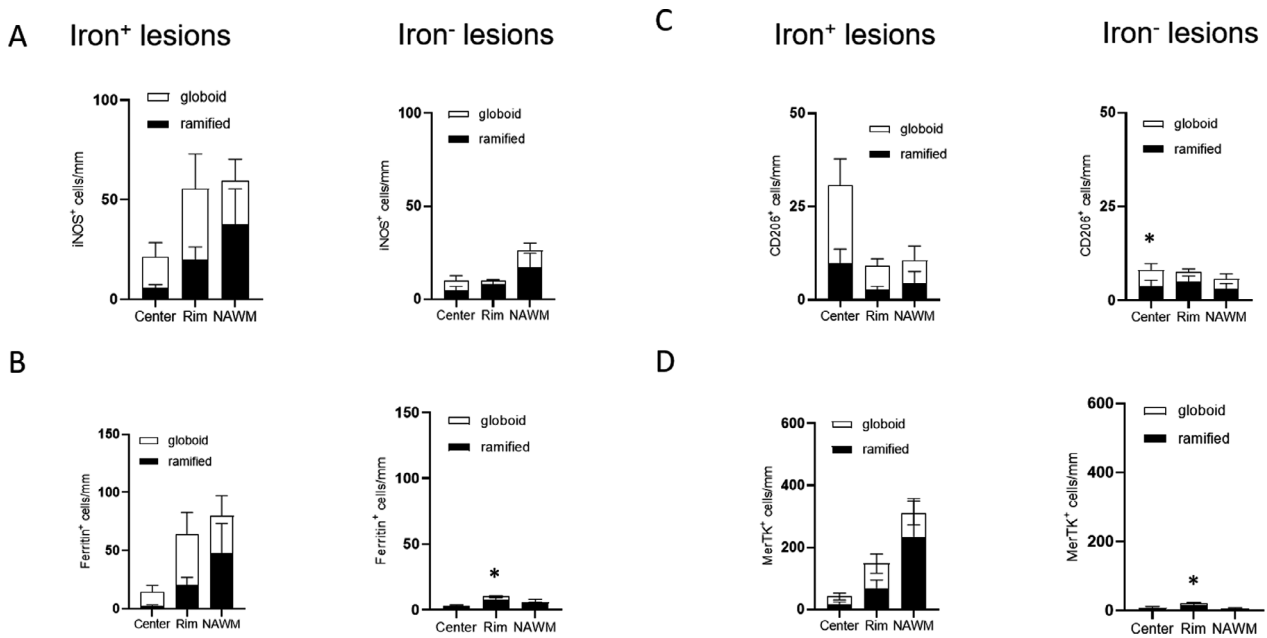


Figure 3. Distribution of activated myeloid cells iron⁺ and iron⁻ lesions. Iron⁺ lesions contain globoid and ramified myeloid cells that express pro-inflammatory (A) iNOS, (B) Ferritin and anti-inflammatory (C) CD206, (D) MerTK markers at higher density as compared to iron⁻ lesions. Bars represent mean + SEM of $n > 10$ ROIs. Total cells in Center, Rim, NAWM were compared between iron⁺ and iron⁻ lesions to determine statistical significance. iNOS, induction of nitric oxide synthase; * $p < 0.05$.

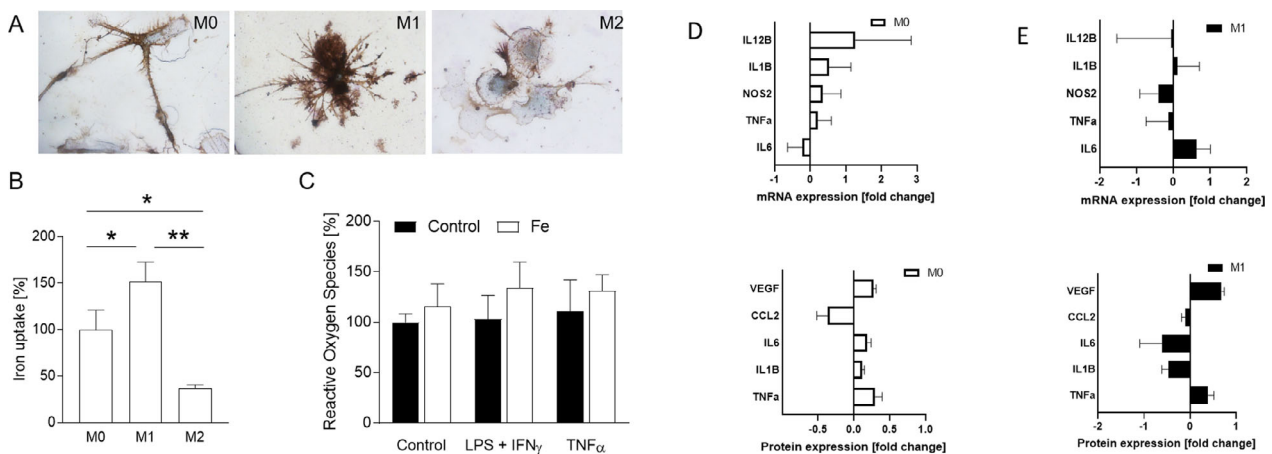


Figure 4. Iron uptake and production of reactive oxygen species in iPSC-derived microglia. (A) M0, M1, and M2 polarized microglia cells (48 h, polarization with IFN γ /LPS (M1) and IL-4 (M2)), stained with Perl's staining after iron(III)sulfate exposure (B) Quantification of polarization-dependent iron uptake by measurement of intracellular radioactive ^{55}Fe . (One-way ANOVA ($F = 21.58$; $p = 0.018$); Tukey–Kramer (M0 vs. M1 $p = 0.0285$; M0 vs M2 $p = 0.0212$; M1 vs. M2 $p = 0.0015$)). (C) CellROX measurements in unstimulated microglia cells, M1-polarized (LPS/IFN γ), and alternatively stimulated cells (TNF α) after 48 h incubation with iron(III)sulfate. (D) mRNA expression levels and (E) protein expression of a panel of inflammation markers in M0 microglia and M1 polarized microglia cells after incubation with iron(III)sulfate (16 and 48 h).

with iron⁺ pan-activated glial cells, suggesting high sensitivity and specificity of this QSM pattern for innate inflammatory activity.

In contrast, high susceptibility puncta within lesions are likely to represent deoxygenated hemoglobin in blood

vessels, as puncta⁺ lesions contained significantly more engorged blood vessels and more fixated blood within the vessels than lesions without punctate susceptibility. Finally, the homogeneous susceptibility in QSM⁺ lesions is likely caused by lesional demyelination. We have

recently shown that denaturation of purified myelin increases its susceptibility to similar levels observed in white matter lesions.²²

The association between susceptibility rims and innate inflammation has been further confirmed in our recent study of MS patients that combined QSM and PET imaging with a radioligand for the microglia and astrocyte activation marker 18 kDa translocator protein (TSPO).²³ We demonstrated that TSPO binding at the lesion rim co-localized with increased susceptibility.

In addition, we have shown in human iPSC-derived microglia that their activation state determines the degree of iron uptake, which was highest in LPS/IFN- γ stimulated, classically activated microglia. Iron uptake, however, did not result in increased production of ROS or proinflammatory cytokines, possibly due to the use of ferric iron rather than the more reactive ferrous iron. This is at variance with previous reports of iron-induced enhanced generation of ROS and TNF in M1-polarized but not in non-polarized or M2-polarized human monocyte-derived macrophages in vitro and in vivo.^{1,24} It has recently become clear that the M1/M2 polarization paradigm is an in vitro concept with no bearing on inflammation in vivo, where myeloid cell phenotypes fall into categories in which M1 and M2 expression profiles have no organizing value.²⁵ Recent single-cell RNA-sequencing data of microglia isolated from five patients with early active MS²⁶ has shed more light on the function of iron⁺ microglia. A microglia subset that is present in MS lesions but not in control-derived microglia, expressed high amounts of *FTH1* and *FTHL*, which encode for the heavy and light subunits of ferritin. This subpopulation also co-expressed APOE, a marker for neurodegenerative microglia²⁷ and low amounts of genes associated with antigen-presentation and phagocytosis, consistent with the minor demyelinating activity in chronic active lesions. A microglia study in Alzheimer's disease demonstrated a similar *FTH1*-expressing microglia phenotype.²⁸

Taken together, our findings suggest that high QSM susceptibility at the rim of white matter lesions is a highly sensitive and specific imaging biomarker for chronic innate inflammatory activity, whereas punctate or low-intensity susceptibility within lesions is not related to inflammation. Our in vitro data further implicate iron as a biomarker for proinflammatory activation of myeloid cells. The clinical relevance of QSM rim lesions for the overall disease course is currently intensely investigated. QSM is highly reproducible²⁹ and can be included in routine clinical MRI protocols for monitoring MS patients. The frequency of high susceptibility rims on QSM or phase imaging in MS patients varies substantially between studies, which is likely due to different MS patient cohorts with differences in disease course and

inflammatory activity. In our study, 12.0% of all T2 lesions were rim positive, which is within the range of previously reported results (1.6% to 32% of the overall T2 lesion load^{1,3,4,30–32}).

Rim-positive lesions have been shown to be more likely to develop tissue damage (T1 black holes)⁴ and slowly expand over time, suggesting a continuous albeit slow demyelinating process.³ The significance of slowly expanding lesions was recently highlighted by reports whereby lesion expansion predicted disability progression and poor clinical outcomes.^{33,34} Moreover, a recent study found that activated microglia in the perilesional white matter, as quantified with TSPO-PET, correlates with MS progression.^{34,35} Given the co-localization of perilesional TSPO binding with QSM signal and the long-lasting presence of increased rim susceptibility, suggests a link between iron⁺ microglia and disease progression. It remains to be demonstrated that QSM rims are more prevalent in progressive MS and that reduction of lesional iron content impacts on disease outcome. Prospective studies that address these questions are currently underway.

Our study has focused on QSM hyperintense white matter lesions; however, we also observed lesions on T2/FLAIR that were QSM isointense (15.2%) or hypointense (27.2%) relative to NAWM. We have previously reported that QSM isointensity occurs in MS patients in Gd-enhancing lesions and in 24.5% of non-enhancing lesions.^{11,14,36} Longitudinal studies suggest that late chronic lesions eventually return to isointense susceptibility.^{11,14} This could represent remyelination although it is improbable that all lesions remyelinate. Similarly, there is no satisfying histopathological explanation for QSM hypointensity in MS lesions, which underlines the need for additional QSM-histology correlative studies.

There are several limitations to this study. While our lesions were a homogeneous population to the degree that they are all derived from periventricular and deep white matter of the cerebrum, we recognize that different lesion locations even within the cerebral white matter may result in different iron content in microglia. In addition, it is possible that activation patterns of iron-positive microglia change with increasing chronicity. Finally, we focused exclusively on lesions that were hyperintense on QSM. We are now conducting additional studies to understand the histopathological changes that result in hypo- or isointense QSM signal.

In summary, our MRI and pathology investigations provide further guidance on how to evaluate QSM hyperintensity signal in cerebral WM lesions of MS patients: QSM hyperintensity in the lesion perimeter is indicative of the presence of inflammatory iron⁺ myeloid cells at the

lesion rim, whereas punctate or low-intensity homogeneous QSM patterns are not associated with inflammation.

Acknowledgments

This work was supported in part by the National Institutes of Health R01NS090464, R01NS105144, S10OD021782 (YW); R01NS102667 (DP) and the National Multiple Sclerosis Society RR-1602-07671 (TDN). This work was made possible through formalin-fixed CNS tissue of MS patients obtained from the Rocky Mountain Multiple Sclerosis Center Tissue Bank.

Conflict of Interest

Yi Wang owns equity in Medimagematic LLC.

Funding Information

This work was supported in part by the National Institutes of Health R01NS090464, R01NS105144, S10OD021782 (YW); R01NS102667 (DP) and the National Multiple Sclerosis Society RR-1602-07671 (TDN). This work was made possible through formalin-fixed CNS tissue of MS patients obtained from the Rocky Mountain Multiple Sclerosis Center Tissue Bank.

References

- Mehta V, Pei W, Yang G, et al. Iron is a sensitive biomarker for inflammation in multiple sclerosis lesions. *PLoS One* 2013;8:e57573.
- Wisnieff C, Ramanan S, Olesik J, et al. Quantitative susceptibility mapping (QSM) of white matter multiple sclerosis lesions: interpreting positive susceptibility and the presence of iron. *Magn Reson Med* 2015;74:564–570.
- Dal-Bianco A, Grabner G, Kronnerwetter C, et al. Slow expansion of multiple sclerosis iron rim lesions: pathology and 7 T magnetic resonance imaging. *Acta Neuropathol* 2017;133:25–42.
- Absinta M, Sati P, Schindler M, et al. Persistent 7-tesla phase rim predicts poor outcome in new multiple sclerosis patient lesions. *J Clin Invest* 2016;126:2597–2609.
- Bagnato F, Hametner S, Yao B, et al. Tracking iron in multiple sclerosis: a combined imaging and histopathological study at 7 Tesla. *Brain* 2011;134(Pt 12):3602–3615.
- de Rochefort L, Liu T, Kressler B, et al. Quantitative susceptibility map reconstruction from MR phase data using bayesian regularization: validation and application to brain imaging. *Magn Reson Med* 2010;63:194–206.
- Langkammer C, Pirpamer L, Seiler S, et al. Quantitative susceptibility mapping in Parkinson's disease. *PLoS One* 2016;11:e0162460.
- Schweitzer AD, Liu T, Gupta A, et al. Quantitative susceptibility mapping of the motor cortex in amyotrophic lateral sclerosis and primary lateral sclerosis. *AJR Am J Roentgenol* 2015;204:1086–1092.
- Dimov AV, Gupta A, Kopell BH, Wang Y. High-resolution QSM for functional and structural depiction of subthalamic nuclei in DBS presurgical mapping. *J Neurosurg* 2018;131:360–367.
- Eskreis-Winkler S, Deh K, Gupta A, et al. Multiple sclerosis lesion geometry in quantitative susceptibility mapping (QSM) and phase imaging. *J Magn Reson Imaging* 2015;42:224–229.
- Zhang S, Nguyen TD, Hurtado Rua SM, et al. Quantitative susceptibility mapping of time-dependent susceptibility changes in multiple sclerosis lesions. *AJNR Am J Neuroradiol* 2019;40:987–993.
- Chawla S, Kister I, Sinnecker T, et al. Longitudinal study of multiple sclerosis lesions using ultra-high field (7T) multiparametric MR imaging. *PLoS One* 2018;13:e0202918.
- Stuber C, Pitt D, Wang Y. Iron in multiple sclerosis and its noninvasive imaging with quantitative susceptibility mapping. *Int J Mol Sci* 2016;17(1):100–121.
- Chen W, Gauthier SA, Gupta A, et al. Quantitative susceptibility mapping of multiple sclerosis lesions at various ages. *Radiology* 2014;271:183–192.
- Liu J, Liu T, de Rochefort L, et al. Morphology enabled dipole inversion for quantitative susceptibility mapping using structural consistency between the magnitude image and the susceptibility map. *NeuroImage* 2012;59:2560–2568.
- Kozlowski C, Weimer RM. An automated method to quantify microglia morphology and application to monitor activation state longitudinally in vivo. *PLoS One* 2012;7:e31814.
- Douvaras P, Sun B, Wang M, et al. Directed differentiation of human pluripotent stem cells to microglia. *Stem Cell Rep* 2017;8:1516–1524.
- Milner R, Campbell IL. The extracellular matrix and cytokines regulate microglial integrin expression and activation. *J Immunol* 2003;170:3850–3858.
- Giles DA, Washnock-Schmid JM, Duncker PC, et al. Myeloid cell plasticity in the evolution of central nervous system autoimmunity. *Ann Neurol* 2018;83:131–141.
- Cai B, Kasikara C, Doran AC, et al. MerTK signaling in macrophages promotes the synthesis of inflammation resolution mediators by suppressing CaMKII activity. *Sci Signal* 2018;11(549):eaar3721.
- Ruddell RG, Hoang-Le D, Barwood JM, et al. Ferritin functions as a proinflammatory cytokine via iron-independent protein kinase C zeta/nuclear factor kappaB-regulated signaling in rat hepatic stellate cells. *Hepatology* 2009;49:887–900.
- Deh K, Ponath GD, Molvi Z, et al. Magnetic susceptibility increases as diamagnetic molecules breakdown: myelin

- digestion during multiple sclerosis lesion formation contributes to increase on QSM. *J Magn Reson Imaging* 2018;48:1281–1287.
23. Kaunzner UW, Kang Y, Zhang S, et al. Quantitative susceptibility mapping identifies inflammation in a subset of chronic multiple sclerosis lesions. *Brain* 2019;142:133–145.
 24. Sindrilaru A, Peters T, Wieschalka S, et al. An unrestrained proinflammatory M1 macrophage population induced by iron impairs wound healing in humans and mice. *J Clin Invest* 2011;121:985–997.
 25. Ransohoff RM. A polarizing question: do M1 and M2 microglia exist? *Nat Neurosci* 2016;19:987–991.
 26. Masuda T, Sankowski R, Staszewski O, et al. Spatial and temporal heterogeneity of mouse and human microglia at single-cell resolution. *Nature* 2019;566:388–392.
 27. Butovsky O, Jedrychowski MP, Cialic R, et al. Targeting miR-155 restores abnormal microglia and attenuates disease in SOD1 mice. *Ann Neurol* 2015;77:75–99.
 28. Olah M, Menon V, Habib N, et al. Single cell RNA sequencing of human microglia uncovers a subset associated with Alzheimer's disease. *Nat Commun* 2020;11:6129.
 29. Deh K, Nguyen TD, Eskreis-Winkler S, et al. Reproducibility of quantitative susceptibility mapping in the brain at two field strengths from two vendors. *J Magn Reson Imaging* 2015;42:1592–1600.
 30. Yao Y, Nguyen TD, Pandya S, et al. Combining quantitative susceptibility mapping with automatic zero reference (QSM0) and myelin water fraction imaging to quantify iron-related myelin damage in chronic active MS lesions. *AJNR Am J Neuroradiol* 2018;39:303–310.
 31. Pitt D, Boster A, Pei W, et al. Imaging cortical lesions in multiple sclerosis with ultra-high-field magnetic resonance imaging. *Arch Neurol* 2010;67:812–818.
 32. Sinnecker T, Schumacher S, Mueller K, et al. MRI phase changes in multiple sclerosis vs neuromyelitis optica lesions at 7T. *Neurol Neuroimmunol Neuroinflamm* 2016;3:e259.
 33. Elliott C, Belachew S, Wolinsky JS, et al. Chronic white matter lesion activity predicts clinical progression in primary progressive multiple sclerosis. *Brain* 2019;142:2787–2799.
 34. Absinta M, Sati P, Masuzzo F, et al. Association of chronic active multiple sclerosis lesions with disability in vivo. *JAMA Neurol* 2019;76(12):1474–1483.
 35. Sucksdorff MMM, Tuisku J, Polvinen E, et al. Brain TSPO-PET predicts later disease progression independent of relapses in multiple sclerosis. *Brain* 2020;143(11):3318–3330.
 36. Zhang Y, Gauthier SA, Gupta A, et al. Quantitative susceptibility mapping and R2* measured changes during white matter lesion development in multiple sclerosis: myelin breakdown, myelin debris degradation and removal, and iron accumulation. *AJNR Am J Neuroradiol* 2016;37:1629–1635.